American Mineralogist, Volume 99, pages 84–93, 2014

Thermal equation of state and spin transition of magnesiosiderite at high pressure and temperature

JIN LIU[1,*], JUNG-FU LIN[1], ZHU MAO[1] AND VITALI B. PRAKAPENKA[2]

[1]Department of Geological Science, Jackson School of Geosciences, The University of Texas at Austin, Austin, Texas 78712, U.S.A.
[2]Consortium for Advanced Radiation Sources, The University of Chicago, Chicago, Illinois 60637, U.S.A.

ABSTRACT

In situ synchrotron X-ray diffraction experiments on natural magnesiosiderite [$(Mg_{0.35}Fe_{0.65})CO_3$] were conducted using resistive and laser-heated diamond-anvil cells (DACs) up to 78 GPa and 1200 K. Based on thermal elastic modeling of the measured pressure-volume curves at given temperatures, we have derived thermal equation of state (EoS) parameters and the spin-crossover diagram of magnesiosiderite across the spin transition. These results show the spin crossover broadened and shifted toward higher pressures at elevated temperatures. Low-spin magnesiosiderite is 6% denser and 8% more incompressible than the high-spin phase at 1200 K and high pressures. Within the spin crossover from 53 to 63 GPa at 1200 K, magnesiosiderite exhibits anomalous thermal elastic behaviors, including a dramatic increase in the thermal expansion coefficient by a factor of 20 and a drop in the isothermal bulk modulus and the bulk sound velocity by approximately 75 and 50%, respectively. Compared with the end-member magnesite [$MgCO_3$] at relevant pressure-temperature conditions of the subducted slabs, the high-spin magnesiosiderite with 65 mol% $FeCO_3$ is approximately 21–23% denser and its unit-cell volume is 2–4% larger, whereas the low-spin state is 28–29% denser and 2% smaller than the end-member magnesite. Since ferromagnesite with 20 mol% of iron has been proposed to be a potential deep-carbon carrier, our results here indicate that the dense low-spin ferromagnesite can become more stable than high-spin ferromagnesite at pressures above approximately 50 GPa, providing a mechanism for (MgFe)-bearing carbonate to be a major carbon host in the deeper lower mantle.

Keywords: Fe-rich carbonate, thermal equation of state, spin transition, ferromagnesite, diamond-anvil cell

INTRODUCTION

The existence of oxidized carbon in the Earth's deep interior can significantly affect several geophysical and geochemical properties of the planet (e.g., Gaillard et al. 2008; Dasgupta and Hirschmann 2010). Due to the nominally low solubility of carbon in the main minerals of the mantle (Keppler et al. 2003; Dasgupta et al. 2013), carbon from primordial origins or altered ocean crusts is expected to be present as accessory phases in the deep mantle, such as carbonates, carbonate melts, carbon-bearing fluids, diamond, and/or iron carbides (e.g., Berg 1986; Alt and Teagle 1999; Pal'yanov et al. 1999). Laboratory studies of carbon-bearing minerals at high pressures and temperatures (*P*-*T*) can provide crucial constraints on the role and behavior of deep carbon in the geochemistry and geophysics of the Earth's mantle, and therefore the mantle's role in the global carbon cycle (Hazen et al. 2012). Magnesite [$MgCO_3$] has been reported to be stable at relevant *P*-*T* conditions of the Earth's lower mantle (Isshiki et al. 2004; Oganov et al. 2008). High *P*-*T* experiments on carbonated peridotite and eclogite further showed that approximately 20 mol% siderite [$FeCO_3$] can be dissolved in magnesite, forming an Fe-bearing [$(MgFe)CO_3$] solid solution with rhombohedral structure (Dasgupta et al. 2004). This form, called ferromagnesite for the Mg-rich part of the system and magnesiosiderite for the Fe-rich part of the system, could be a stable major deep-carbon host in the lower mantle.

Iron as a transition metal is known to play an important role in the physical, chemical, and transport properties of the mantle minerals due to the various electronic spin and valence states exhibited by the 3*d* electrons of iron at high *P*-*T* conditions (e.g., Lin and Tsuchiya 2008). An electronic high-spin (HS) to low-spin (LS) transition of iron in the magnesite-siderite system has been recently observed to occur at approximately 45 GPa using several experimental and theoretical techniques including high-pressure X-ray emission spectroscopy, X-ray diffraction, laser Raman spectroscopy, and first-principles calculations (Mattila et al. 2007; Shi et al. 2008; Lavina et al. 2009, 2010a, 2010b; Nagai et al. 2010; Farfan et al. 2012; Lin et al. 2012). This transition is associated with a 6–10% reduction in the unit-cell volume, making the LS state denser and more incompressible than the HS counterpart (Lavina et al. 2009, 2010b; Nagai et al. 2010; Farfan et al. 2012; Lin et al. 2012). It has been suggested that iron may preferentially partition into the LS ferromagnesite, which would make it a stable deep-carbon host in the lower mantle (Lavina et al. 2009, 2010a, 2010b; Nagai et al. 2010; Farfan et al. 2012; Lin et al. 2012). On the other hand, iron-bearing magnesite and siderite have been reported to transform into an assemblage of magnetite, nano-diamonds, and a new high-pressure phase with three-membered rings of corner-sharing $(CO_4)^{4-}$ tetrahedra at pressures exceeding 40 GPa and high temperatures (Boulard et al. 2011, 2012). Furthermore, the electronic spin-pairing transi-

* E-mail: jinliu@utexas.edu

0003-004X/14/0001–084$05.00/DOI: http://dx.doi.org/10.2138/am.2014.4553

tion of Fe^{2+} and its associated effects on the thermal EoS of the magnesite-siderite system have only been previously investigated at high pressures and room temperature.

Spin transitions of ferric and ferrous iron and their associated effects have also been reported to occur in other iron-bearing mantle minerals at high pressures, including ferropericlase, perovskite, and post-perovskite [see Lin and Tsuchiya (2008) and Lin et al. (2013) for recent reviews]. In particular, the spin transition of iron has been observed to affect several physical and chemical properties of ferropericlase including density, incompressibility, sound velocities, and transport properties (Lin et al. 2005, 2006, 2007a; Tsuchiya et al. 2006; Fei et al. 2007b; Speziale et al. 2007; Crowhurst et al. 2008; Marquardt et al. 2009a, 2009b; Wentzcovitch et al. 2009; Wu et al. 2009; Komabayashi et al. 2010; Mao et al. 2011). Recent theoretical and experimental studies also show that the spin transition becomes a broad, continuous spin crossover at high *P-T* conditions (Tsuchiya et al. 2006; Lin et al. 2007b; Wentzcovitch et al. 2009; Wu et al. 2009; Komabayashi et al. 2010; Mao et al. 2011). Along a typical mantle geotherm (Brown and Shankland 1981), the spin crossover in ferropericlase is expected to occur approximately between 1700 and 2700 km depth (e.g., Mao et al. 2011). Therefore, studying the spin transition and its associated effects on thermal EoS parameters in the magnesite-siderite system at relevant *P-T* conditions of the Earth's mantle would help us understand the nature of the spin crossover as well as the characteristics of this potential deep-carbon host.

In the present work, we have carried out synchrotron X-ray diffraction measurements on magnesiosiderite [$(Mg_{0.35}Fe_{0.65})CO_3$] in an externally heated diamond-anvil cell (EHDAC) or a laser-heated diamond-anvil cell (LHDAC) at high *P-T* conditions to understand its thermal EoS parameters across the spin crossover. We used the *P-V-T* relations of magnesiosiderite to model the spin-crossover diagram up to 80 GPa and 1200 K and to derive thermal EoS parameters for HS, LS, and mixed-spin states, respectively. The modeled spin-crossover diagram of magnesiosiderite shows that increasing temperature broadens the width of the spin crossover toward higher pressures. These results are applied to decipher the role of magnesiosiderite in the lower-mantle deep-carbon storage.

Experimental methods

A natural single-crystal magnesiosiderite from Brazil was used as the starting material, which has also been previously studied by Lin et al. (2012) using optical Raman and synchrotron X-ray diffraction spectroscopies at high pressures and room temperature. Briefly, electron microprobe and XRD analyses showed that the sample is chemically homogeneous within analytical uncertainties, and has a composition $(Mg_{0.33}Mn_{0.02}Fe_{0.65})CO_3$ with lattice parameters $a = 4.6753(12)$ Å and $c = 15.2794(30)$ Å; for simplicity, the composition of the sample is referred to as $(Mg_{0.35}Fe_{0.65})CO_3$ by ignoring the manganese content and by keeping the amount of iron fixed. Visual observations using a high-magnification optical microscope showed that the single-crystal sample was optically homogenous without any signs of chemical inclusions or variations in color. High *P-T* X-ray diffraction experiments were conducted at 13IDD beamline of the GSECARS of the Advanced Photon Source (APS), Argonne National Laboratory (ANL), using a monochromatic X-ray beam with a wavelength of 0.3344 Å. Single-crystal or powder X-ray diffraction (XRD) measurements were performed using an EHDAC (Kantor et al. 2012) or an LHDAC (Prakapenka et al. 2008). A MarCCD detector was used to collect two-dimensional XRD images that were processed and integrated using Fit2D software (Hammersley et al. 1996). The tilting and rotation of the MarCCD detector relative to the incident X-ray beam were calibrated using cerium dioxide (CeO_2) powder as the X-ray diffraction standard. The sample-detector distance was calculated from the powder CeO_2 diffraction pattern at ambient conditions.

For the EHDAC experiments, both powder and single-crystal XRD measurements were performed using Ne as the pressure medium. For the single-crystal experiments, a piece of the single-crystal magnesiosiderite was cleaved from the natural crystal along the (101) plane and loaded into an EHDAC, together with a 5 μm pellet of Au powder as the pressure calibrant (Fei et al. 2007a). A K-type thermocouple was attached to the pavilion of the diamond, approximately 500 μm away from its culet, and used to monitor the temperature. For the powder runs, powdered magnesiosiderite was mixed with 3 wt% micro-sized Au powder as the pressure calibrant (Fei et al. 2007a) by mechanically grinding the mixture for approximately 4 h. Subsequently, the mixture was slightly pressed between two opposing diamond anvils to form an approximately 15 μm thick disk. The powder sample disk was loaded into an EHDAC with 300 μm culets and a Re gasket, which was pre-indented to 30 μm thick and had a drill hole of 150 μm diameter.

Two runs of the LHDAC experiments were conducted using the double-sided Nd:YLF laser heating system at GSECARS (Prakapenka et al. 2008). The aforementioned powder sample disk was sandwiched between two dried NaCl disks, which functioned as the thermal insulator and pressure medium, in a symmetric DAC with 300 or 200 μm culets and a Re gasket. To remove any potential air and moisture contamination in the sample chamber, the sandwiched sample assemblage was evacuated for 30 min before closing the sample chamber in vacuum using the high-pressure gas loading system in the Mineral Physics Laboratory of the University of Texas at Austin. Two infrared laser beams were focused down to 25 μm diameter on both sides of the sample, and were co-axially aligned with the incoming X-ray beam using the X-ray induced luminescence on the sample and NaCl (Prakapenka et al. 2008). Temperatures of the heated samples were determined by fitting the measured thermal radiation spectra assuming the Graybody approximation (Prakapenka et al. 2008). The uncertainty of temperatures (1σ) was ±50 K based on multiple temperature measurements from both sides of the laser-heated sample. Pressures were calculated from in situ XRD patterns of the Au standard (Fei et al. 2007a).

Results and data analyses

XRD patterns of the sample were collected at five temperatures (300, 450, 600, 750, and 1200 K) in 1–3 GPa intervals up to 78 GPa (Figs. 1 and 2); data at 1200 K were taken from the LHDAC experiments while all other high-temperature points were obtained from the EHDAC experiments. We limited the laser heating temperature to 1200 K because Fe-rich magnesiosiderite has been reported to transform into a new Fe^{3+}-bearing high-pressure phase at temperatures above 1850 K and high pressures (Boulard et al. 2011, 2012). The unit-cell parameters of the magnesiosiderite and Au in this study were calculated using 3–8 diffraction lines, respectively, at high *P-T* (Fig. 3). Analyses of the XRD patterns from heated and quenched sample assemblages only showed diffraction peaks from the sample, Au calibrant, and Ne or NaCl medium, indicating that the sample remained stable in the rhombohedral structure and that no dissociation or chemical reaction had occurred in the sample during high *P-T* experiments (Figs. 1 and 2). All error bars reported here are derived from standard error propagations and represent ±1σ.

The compression curve of $(Mg_{0.35}Fe_{0.65})CO_3$ at 300 K shows a dramatic volume reduction of 6.5% over a pressure interval of ~4 GPa from 43.4(4) to 47.5(5) GPa, consistent with the spin transition pressure reported previously (Mattila et al. 2007; Shi et al. 2008; Lavina et al. 2009, 2010a, 2010b; Nagai et al. 2010; Farfan et al. 2012; Lin et al. 2012). The *P-V* curves at given high temperatures clearly show an increase in the onset pressure and the width of the volume reduction; i.e., the volume reduction at 1200 K starts at 53.2(5) GPa and ends at 63.0(5) GPa over a pressure interval of approximately 10 GPa (Fig. 3). The *P-V-T* curves were used to derive thermal EoS parameters of the HS, LS, and mixed-spin states as well as the spin-crossover diagram of the magnesiosiderite.

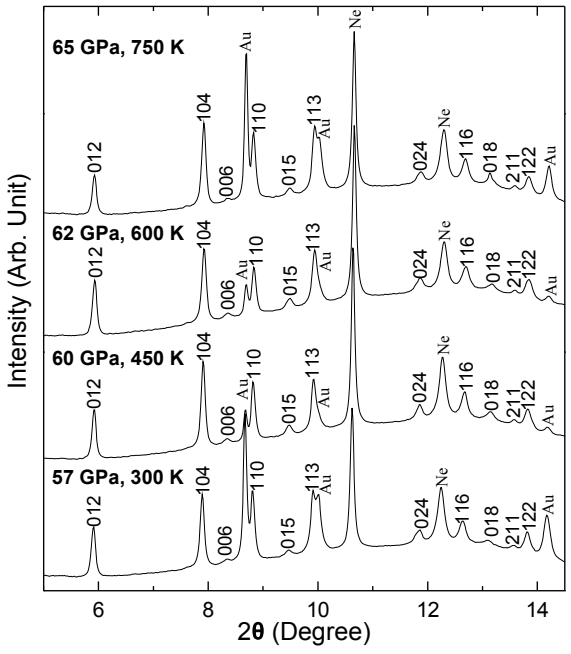

FIGURE 1. Representative X-ray diffraction patterns of magnesiosiderite [$(Mg_{0.35}Fe_{0.65})CO_3$] measured from an EHDAC. Gold (Au) was used as the internal pressure calibrant (Fei et al. 2007a), while neon (Ne) was used as the thermal insulator and pressure medium. The wavelength of the monochromatic X-ray beam was 0.3344 Å.

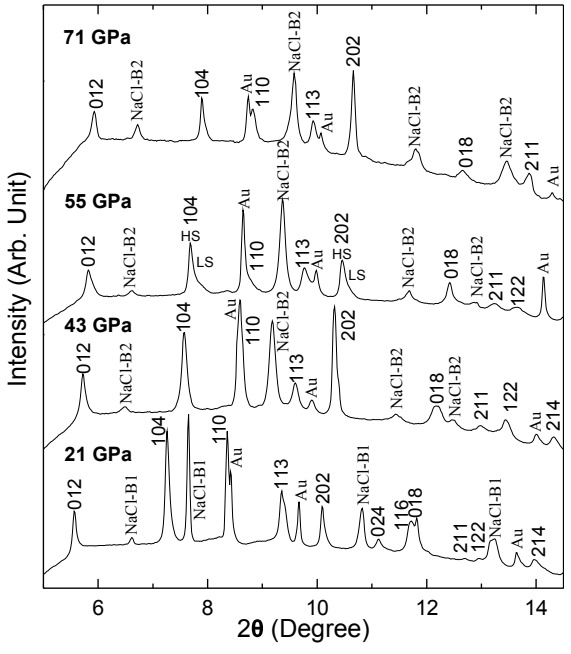

FIGURE 2. Representative X-ray diffraction patterns of magnesiosiderite [$(Mg_{0.35}Fe_{0.65})CO_3$] at high pressures and 1200 K measured from a LHDAC. HS and LS states are labeled to illustrate the splitting of the diffraction peaks across the spin transition. Gold (Au) was used as the internal pressure calibrant (Fei et al. 2007a), while sodium chloride (NaCl) in B1 or B2 structure was used as the thermal insulator and pressure medium. The wavelength of the monochromatic X-ray beam was 0.3344 Å.

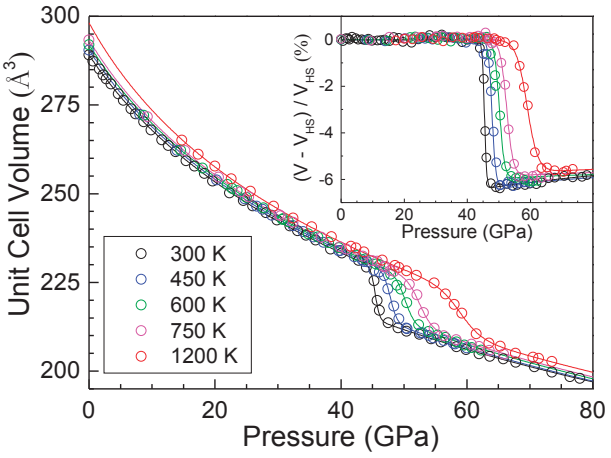

FIGURE 3. Pressure-volume relations of magnesiosiderite [$(Mg_{0.35}Fe_{0.65})CO_3$] at high *P-T*. Open circles: experimental measurements; lines: modeled results. The insert figure shows the volume difference between experimental results and the HS state reference. (Online color.)

Equation of state at room temperature

The *P-V* curve of the sample at 300 K up to 40 GPa (before the abnormal volume reduction) was fitted to a third-order Birch-Murnaghan EoS (BM EoS) to derive the unit-cell volume (V_0), the bulk modulus (K_0) and the pressure derivative of the bulk modulus (K_0') at ambient conditions using the EosFit v5.2 programs (Birch 1978; Angel 2000), yielding V_0 = 289.2(1) Å^3, K_0 = 109(1) GPa, and K_0' = 4.9(2) for the HS state (Table 1). To identify the onset pressure for the occurrence of the LS state (P_{LS}) and the ending pressure for the HS state (P_{HS}), our experimental data were compared with the modeled *P-V* curve for the HS state (Speziale et al. 2007; Mao et al. 2011)—the P_{LS} and P_{HS} can thus be determined from the variation in the volume difference between the experimental *P-V* data and the modeled HS *P-V* curve (Fig. 3 insert), yielding P_{LS} = 43.4(4) GPa and P_{HS} = 47.5(5) GPa, with a width of 4.1(9) GPa. Additionally, EoS parameters for the LS magnesiosiderite were obtained from fitting the *P-V* data between 47.5 and 78 GPa with the third-order BM EoS (Table 2). The derived V_0, K_0, and K_0' values for the HS and LS states at 300 K are in good agreement with previous reports (Lavina et al. 2009, 2010a, 2010b; Nagai et al. 2010; Farfan et al. 2012; Lin et al. 2012).

Thermal equation of state parameters

For *P-V* data at elevated temperatures, the third-order isothermal BM EoS was employed to derive the thermal EoS parameters for the HS and LS states using the EosFit v5.2 programs (Birch 1978; Angel 2000):

$$P(V,T)=\frac{3K_{0T}}{2}\left[\left(\frac{V_{0T}}{V}\right)^{\frac{7}{3}}-\left(\frac{V_{0T}}{V}\right)^{\frac{5}{3}}\right]\left\{1+\frac{3}{4}\left(K_{0T}^{'}-4\right)\left[\left(\frac{V_{0T}}{V}\right)^{\frac{7}{3}}-1\right]\right\}$$

where 0*T* denotes ambient pressure and a given high temperature, respectively. Neglecting higher-order pressure derivatives of the bulk modulus and assuming that K_{0T}' is a constant in the temperature range of our study (Zhang et al. 1998), the K_{0T} can be determined using the following equation:

TABLE 1. Thermal elastic parameters of the Fe-bearing magnesite [(MgFe)CO_3] in the high-spin state at ambient conditions

Reference	Composition	V_0 (Å^3)	K_{0T} (GPa)	K_T'	$(\partial K_T/\partial T)_{0P}$ (GPa/K)	α_0 (10^{-5} K^{-1})	α_1 (10^{-8} K^{-2})
This study	$(Fe_{0.65}Mg_{0.33}Mn_{0.02})CO_3$	289.2 (1)	109 (1)	4.9 (2)	–0.026 (2)	2.8(2)	0.9(3)
Lin et al. (2012)	$(Fe_{0.65}Mg_{0.33}Mn_{0.02})CO_3$	289.1 (1)	108 (2)	4.8 (2)			
Lavina et al. (2010b)	$(Fe_{0.96}Mg_{0.04})CO_3$	294.4 (3)	110 (2)	4.6 (2)			
Lavina et al. (2010a)	$(Mg_{0.87}Fe_{0.12}Ca_{0.01})CO_3$	281.0 (5)	102.8 (3)	5.44			
Nagai et al. (2010)	$(Fe_{0.73}Mg_{0.22}Mn_{0.05})CO_3$	293.5 (1)	120 (3)	4.3			
Zhang et al. (1998)	$(Fe_{0.998}Mn_{0.002})CO_3$	292.83 (4)	117 (1)	4[a]	–0.031(3)	1.8(4)	3.5(6)
Zhang et al. (1998)	$(Fe_{0.60}Mg_{0.38}Mn_{0.02})CO_3$	288.3 (1)	112 (1)	4[a]	–0.026(2)	2.1(2)	3.0(4)
Litasov et al. (2008)	$(Mg_{0.975}Fe_{0.015}Mn_{0.006}Ca_{0.004})CO_3$	279.55 (2)	97.1 (5)	5.44(7)	–0.013(1)	4.03(7)	0.5(1)
Isshiki et al. (2004)	$(Mg_{0.994}Ca_{0.006})CO_3$		103 (2)	5			
Fiquet et al. (2002)	$MgCO_3$	279.2 (2)	108 (3)	5.0 (2)			
Zhang et al. (1997)	$MgCO_3$	279.3 (2)	103 (1)	4[a]	–0.021(2)	3.15(17)	2.3(3)

Notes: The thermal equation of state parameters were derived using the Birch-Murnaghan EoS when possible (Birch 1978). Literature values were refitted with the linear function for the thermal expansion coefficients in order to have more consistent systematic comparisons. Error bars represent one standard deviation in experimental uncertainties in our study. [a] = Fixed at 4 with an error of ±0.10.

TABLE 2. Thermal elastic parameters of the low-spin magnesiosiderite

Reference	Composition	V_0 (Å^3)	K_{0T} (GPa)	K_T'	$(\partial K_T/\partial T)_{0P}$ (GPa/K)	α_0 (10^{-5} K^{-1})	α_1 (10^{-8} K^{-2})
This study (LS)	$(Fe_{0.65}Mg_{0.33}Mn_{0.02})CO_3$	265(3)	125(3)	5.3(2)	–0.023 (5)	2.3(2)	0.14(9)
Lin et al. (2012)	$(Fe_{0.65}Mg_{0.33}Mn_{0.02})CO_3$	267(2)	127(5)	5.1(2)			
Lavina et al. (2009)	$(Fe_{0.72}Mg_{0.24}Mn_{0.03}Ca_{0.01})CO_3$	263(3)	148(12)	5			

Notes: The thermal equation of state parameters were derived using the Birch-Murnaghan EoS (Birch 1978). Error bars represent one standard deviation in experimental uncertainties in our study.

$$K_{0T} = K_0 + (\partial K_T / \partial T)_{0P}(T - 300)$$

where $(\partial K_T/\partial T)_{0P}$ is the temperature derivative of the bulk modulus at ambient pressure. The $(\partial K_T/\partial T)_{0P}$ is found to be a constant within the temperature range of our study. The zero-pressure unit-cell volume (V_{0T}) at an elevated temperature T is expressed as

$$V_{0T} = V_0 \exp \int_{300}^{T} \alpha_T \, dT$$

where α_T is the thermal expansion coefficient at high temperature and ambient pressure. In our model here, α_T is assumed to be a linear function of temperature:

$$\alpha_T = \alpha_0 + \alpha_1 T$$

where α_0 and α_1 are constants. We have also modeled the thermal expansion coefficient using a second-order polynomial function, instead of the above linear function, but the second-order constant is found to be statistically insignificant at the 2σ confidence level to justify the use of the polynomial function within our limited temperature range.

The modeled *P-V-T* curves for the HS state were then used as the reference for derivation of the P_{LS} and P_{HS} using the variation in the volume difference between the modeled results and experimental data at high *P-T* (Fig. 3 insert). Thermal EoS parameters of the LS state can then be determined using the same aforementioned procedure. These analyses show that the HS state exhibits $(\partial K_T/\partial T)_{0P}$ = –0.026(2) GPa/K and α (K^{-1}) = 2.8(2) × 10^{-5} + 0.9(3) × 10^{-8} *T* (Table 1), while the LS state has $(\partial K_T/\partial T)_{0P}$ = –0.023(5) GPa/K and α (K^{-1}) = 2.3(2) × 10^{-5} + 0.14(9) × 10^{-8} *T* (Table 2).

Spin-crossover diagram

The *P-V-T* relations of the magnesiosiderite were used to derive the fraction of the HS and LS states for constructing the spin-crossover diagram. Following the thermodynamic methods described previously (Tsuchiya et al. 2006; Speziale et al. 2007; Wentzcovitch et al. 2009; Mao et al. 2011), the unit-cell volume of the sample within the spin crossover was treated as an ideal solid-solution mixture of the HS and LS states

$$V = n_{LS} V_{LS} + (1 - n_{LS}) V_{HS}$$

where V_{HS} and V_{LS} are the unit-cell volume of the HS and LS states, respectively, and n_{LS} is the LS fraction. With the experimentally determined n_{LS} at a given temperature (Fig. 4), the LS fraction of the magnesiosiderite at a given *P-T* condition was modeled using the Gibbs free energy difference between the LS and HS states ($\Delta G_{LS\text{-}HS}$) across the spin crossover (Tsuchiya et al. 2006; Speziale et al. 2007; Wentzcovitch et al. 2009):

$$n_{LS} = 1 / \left[1 + \exp(\Delta G_{LS\text{-}HS} / T)\right]$$

Here the *P-T* dependence of the $\Delta G_{LS\text{-}HS}$ is expressed using the following empirical relation:

$$\Delta G_{LS\text{-}HS} = b_0 + b_1 (P - P_{HS}) / (P_{LS} - P_{HS})$$

where b_0 and b_1 are two temperature-dependent constants, and P_{LS} and P_{HS} are the onset pressure for the occurrence of the LS state and the ending pressure for the HS state, respectively. Parameters b_0 and b_1 are derived from the non-linear least-square fit of the experimentally determined n_{LS} as a function of *P-T*. We note that this model has been successfully applied to derive the spin-crossover diagram of the lower-mantle ferropericlase using experimentally measured thermal *P-V-T* data (Mao et al. 2011). Using the derived width of the spin transition and thermal EoS parameters of the magnesiosiderite, the fraction of the LS state and the spin-crossover diagram can be derived from modeling our data between 300 and 1200 K at high pressures (Figs. 4 and 5). The spin-crossover diagram shows apparently positive values for the effective d*P*/d*T* of the transition boundaries and the width of the spin crossover widens at higher temperatures (Fig. 5).

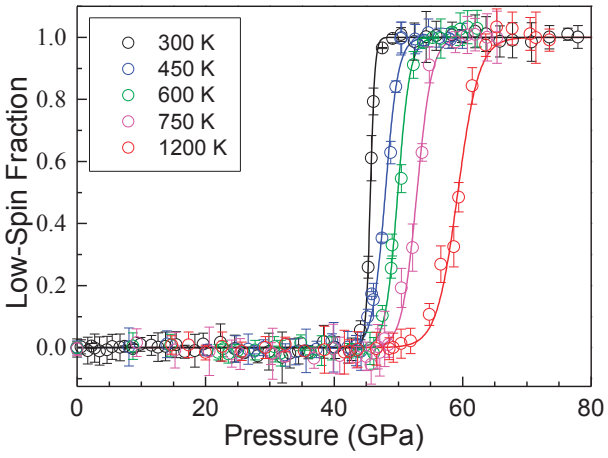

FIGURE 4. Low-spin fraction of magnesiosiderite [$(Mg_{0.35}Fe_{0.65})CO_3$] as a function of pressure compared with the fitting results. Open circles: experimental measurements; lines: fitting results. Vertical ticks represent the error for the low-spin fraction. Errors are calculated using standard error propagations from our modeled parameters. (Online color.)

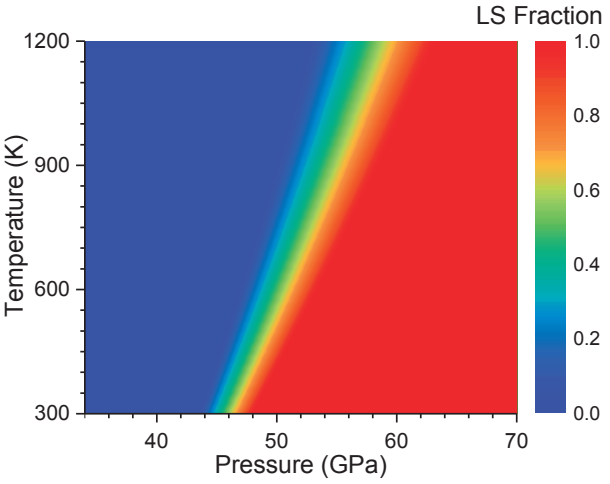

FIGURE 5. Spin crossover of iron in magnesiosiderite [$(Mg_{0.35}Fe_{0.65})CO_3$] at high *P-T*. The color bar on the right represents the fraction of the LS state. (Online color.)

Thermal elastic properties along an isotherm

Using the obtained thermal EoS parameters and the LS fraction, thermoelastic properties of the magnesiosiderite, including thermal expansion coefficient (α), isothermal bulk modulus (K_T), and bulk sound velocity (V_Φ), have also been derived at given temperatures (300, 450, 600, 750, and 1200 K) and high pressures up to 80 GPa across the spin crossover (Figs. 6 and 7). The thermal expansion coefficient across the transition is defined as (Mao et al. 2011):

$$\alpha = \frac{1}{V}\frac{\partial V}{\partial T} = \frac{1}{V}\frac{\partial[n_{LS}V_{LS} + (1-n_{LS})V_{HS}]}{\partial T}.$$

The isothermal bulk modulus is calculated using the equation (Wentzcovitch et al. 2009):

$$\frac{V}{K_T} = n_{LS}\frac{V_{LS}}{K_{LS}} + (1-n_{LS})\frac{V_{HS}}{K_{HS}} - (V_{LS}-V_{HS})\left(\frac{\partial n_{LS}}{\partial P}\right)_T$$

where K_{HS} and K_{LS} are the isothermal bulk modulus of the HS and LS state at a given *P-T* condition, respectively. The last term accounts for the pressure-dependent LS fraction that can affect the modulus as a result of the anomalous volume reduction (V_{LS}-V_{HS}) across the transition (Fig. 6b) (Wentzcovitch et al. 2009). With the derived K_T and α, the bulk sound velocity (V_Φ) can be calculated using the equations:

$$V_\Phi = \sqrt{K_S/\rho}$$

$$K_S = (1+\alpha\gamma T)K_T$$

where K_S is the adiabatic bulk modulus, ρ is density, and γ is the thermodynamic Grüneisen parameter. Because the γ value of the sample at high *P-T* remains unknown across the spin transition, we used the following equation to calculate the γ value at ambient conditions and assume it remains a constant at high *P-T*

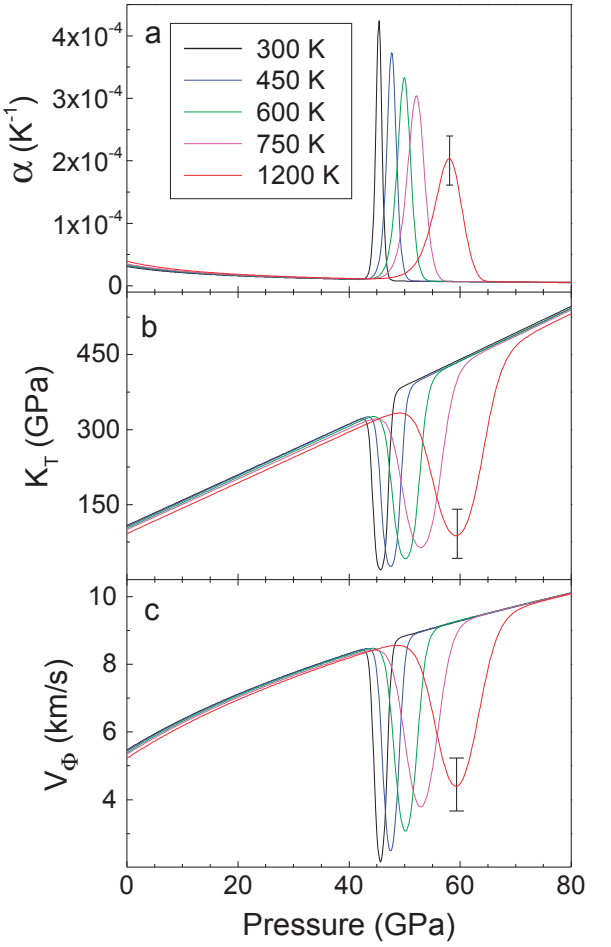

FIGURE 6. Thermal elastic parameters of magnesiosiderite [$(Mg_{0.35}Fe_{0.65})CO_3$] at constant temperatures. α = thermal expansion coefficient; K_T = isothermal bulk modulus; V_Φ = bulk sound velocity. Vertical ticks = representative errors (±1σ) for α, K_T, and V_Φ, respectively. (Online color.)

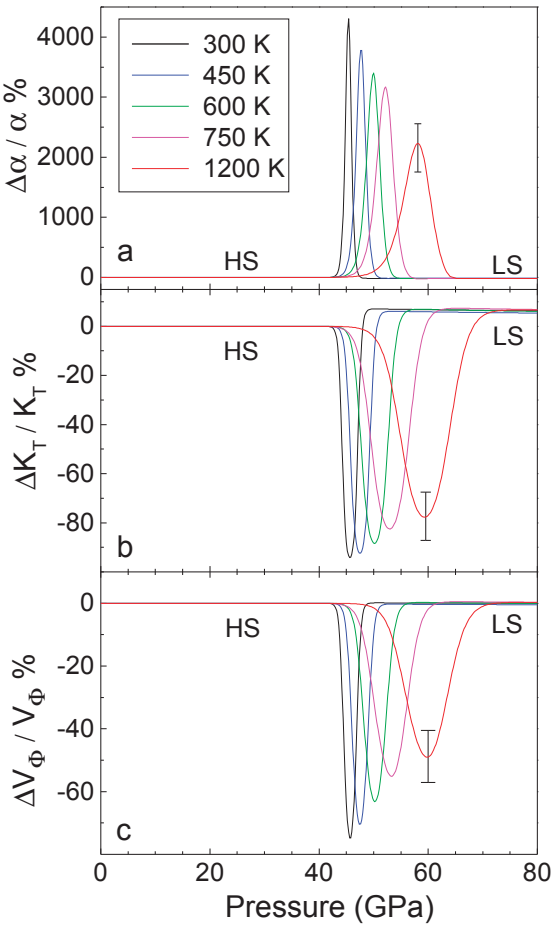

FIGURE 7. Variations of thermal elastic parameters for the LS magnesiosiderite at constant temperatures using the HS state as the reference. α = thermal expansion coefficient; K_T = isothermal bulk modulus; V_Φ = bulk sound velocity. Vertical ticks = representative errors. (Online color.)

$$\gamma = \frac{\alpha K_S}{\rho C_P}$$

where K_S is the adiabatic bulk modulus and C_P is the heat capacity at constant pressure. Using the values of $\alpha = 3.08 \times 10^{-5}$ K^{-1} (this study), K_S = 113.4 GPa (Sanchez-Valle et al. 2011), ρ = 3.654 g/cm^3 (this study), and C_P = 82.44 J/(mol·K) (Robie et al. 1984) at 300 K, the calculated γ value is 1.2(1).

DISCUSSIONS AND IMPLICATIONS

Spin crossover at high *P-T*

The modeled spin-crossover diagram of the magnesiosiderite shows an extended crossover behavior at high temperatures with an apparently positive value for the effective d*P*/d*T* of approximately 10 MPa/K (Fig. 5). Specifically, the width of the transition is approximately 4 GPa at 300 K but expands to approximately 10 GPa at 1200 K. The onset pressure for the occurrence of the LS state increases from 43.4(4) GPa at 300 K to 53.2(5) GPa at 1200 K (Fig. 8). Such spin-crossover behavior has been previously reported to occur in ferropericlase theoretically and experimentally (Tsuchiya et al. 2006; Lin et al. 2007b; Wentzcovitch et al. 2009; Wu et al. 2009; Komabayashi et al. 2010; Mao et al. 2011). Compared with ferropericlase, the spin crossover in magnesiosiderite remains much narrower and occurs at relative lower pressures (Figs. 5 and 8). The relatively sharp spin crossover in the $MgCO_3$-$FeCO_3$ system is likely a result of the localized FeO_6 octahedra that are more isolated and separated from other iron ions in the surrounding FeO_6 octahedra (Lavina et al. 2010b). Previous theoretical and experimental studies on ferropericlase [(MgFe)O] (e.g., Wentzcovitch et al. 2009; Mao et al. 2011) have reported apparently positive values for the effective d*P*/d*T* slope. At a given temperature, the spin transition is reported to be a pressure-induced volume-driven transition in which the pressure-induced volume reducution increases the crystal-field splitting energy that eventually overcomes the spin-pairing energy (e.g., Burns 1993; Persson et al. 2006).

We note that the presence of nonhydrostaticity and pressure gradient in the sample chamber may cause a broadening in the width of the spin crossover (Lin and Tsuchiya 2008). In this study, the use of Ne pressure medium and the tightly focused X-ray beam of less than 5 μm in diameter (FWHM) would minimize the influence of these factors. Therefore, the broadening of the spin crossover at higher *P-T* can be treated as an intrinsic property of the Fe^{2+} ions in magnesiosiderite at elevated temperatures, in which high temperature provides higher configuration entropy to stablize the mixture of the HS and LS states (Burns 1993; Tsuchiya et al. 2006). Previous studies have shown that the HS state is favored at higher temperatures due to the larger entropy for Fe^{2+} in the octahedral site via the thermal expansion effect (Li 2007; Wentzcovitch et al. 2009). Consequently, additional compression (smaller unit-cell volume) is necessary for the LS state to become stable at elevated temperatures.

Compositional effects on the spin transition pressure

To illustrate the compositional effect on the transition pressure and thermal EoS parameters in the $MgCO_3$-$FeCO_3$ system as well as MgO-FeO system, we have plotted our results and literature transition pressures (Fig. 9) for comparison (Badro et al. 2003; Speziale et al. 2005; Lin et al. 2005, 2006, 2007b, 2012; Keppler et al. 2007; Fei et al. 2007b; Crowhurst et al. 2008; Lavina et al. 2009, 2010a, 2010b; Komabayashi et al. 2010; Nagai et al. 2010; Mao et al. 2011; Farfan et al. 2012). Among all iron-bearing earth minerals, we note that the spin transitions in these two systems have been most extensively documented using high-pressure X-ray and laser optical spectroscopic techniques. The transition in the $MgCO_3$-$FeCO_3$ system occurs at 45(5) GPa without observable compositional effects (Mattila et al. 2007; Shi et al. 2008; Lavina et al. 2009, 2010a, 2010b; Nagai et al. 2010; Farfan et al. 2012; Lin et al. 2012). That is, the substitution of Fe^{2+} ions for Mg^{2+} ions in $MgCO_3$ does not show any appreciable effect on the spin transition pressure. This can be used to support the solid-solution model that we used to derive the spin fraction as a function of the volume reduction. In the (MgFe)O system, on the other hand, the transition pressure generally increases from 40–50 GPa for MgO-rich part (ferropericlase) to approximately 102 GPa for FeO-rich part (magnesiowustite) (Badro et al. 2003; Speziale et al. 2005; Lin et al. 2005, 2006, 2007b; Persson et

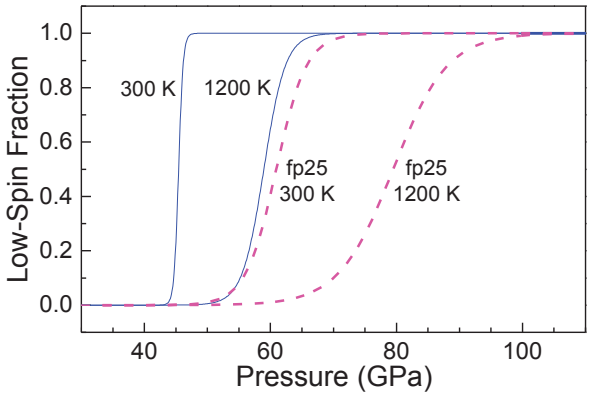

FIGURE 8. Comparison of the low-spin fraction between magnesiosiderite and ferropericlase at high *P-T*. Solid lines = magnesiosiderite; dashed lines = ferropericlase [$(Mg_{0.75}Fe_{0.25})O$; fp25] (Mao et al. 2011). (Online color.)

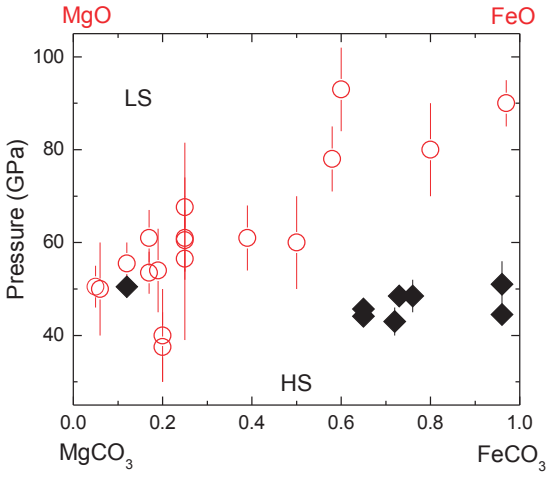

FIGURE 9. Comparison of the spin transition pressures in (MgFe)CO_3 and (MgFe)O solid solution systems. Solid diamonds = (MgFe)CO_3 (Lavina et al. 2009, 2010a, 2010b; Nagai et al. 2010; Farfan et al. 2012; Lin et al. 2012); open circles = (MgFe)O (Badro et al. 2003; Speziale et al. 2005; Lin et al. 2005, 2006, 2007b; Keppler et al. 2007; Fei et al. 2007b; Crowhurst et al. 2008; Komabayashi et al. 2010; Mao et al. 2011). (Online color.)

al. 2006; Keppler et al. 2007; Fei et al. 2007b; Crowhurst et al. 2008; Komabayashi et al. 2010; Mao et al. 2011), indicating a strong compositional effect that stabilizes the high-spin state. These analyses indicate that the Fe^{2+}-Fe^{2+} exchange interaction in the (MgFe)O system plays a more significant role in the spin transition than that in the (MgFe)CO_3 system (Figs. 8 and 9) (Lin et al. 2006).

Abnormal thermal EoS and stability of (MgFe)CO_3

Previous studies on the EoS of (MgFe)CO_3 have shown that the spin transition of iron causes approximately 6–10% volume reduction from the HS state to the LS state in magnesiosiderite containing more than 65% iron (Lavina et al. 2009, 2010b; Nagai et al. 2010; Farfan et al. 2012; Lin et al. 2012). However, thermal EoS parameters within the spin transition remain unclear at high *P-T*. Our thermoelastic modeling of the *P-V-T* relations of the magnesiosiderite shows abnormal behavior in the thermal expansion coefficient, isothermal bulk modulus, and bulk sound velocity within the spin transition (Figs. 6 and 7). Specifically, within the transition, the thermal expansion coefficient increases by approximately a factor of 40 at 300 K and 20 at 1200 K, whereas the isothermal bulk modulus and the bulk sound velocity decrease by approximately 75 and 50% at 1200 K, respectively. It should be noted that such abnormal behaviors within the spin transitions have been reported for the lower-mantle ferropericlase (Speziale et al. 2007; Crowhurst et al. 2008; Wentzcovitch et al. 2009; Wu et al. 2009; Mao et al. 2011). In comparison to the lower-mantle ferropericlase, our magnesiosiderite sample exhibits similar abnormal behaviors across the spin transition, although the magnitude of the changes was much higher than that of ferropericlase as a result of the larger volume reduction across the sharper spin transition at high *P-T*.

The spin transition increases the isothermal bulk modulus by approximately 10% and decreases the thermal expansion coefficient by nearly 20%, making the LS state much more incompressible and less expandable than the HS state. The effects of the spin transition on the bulk modulus can be understood in terms of the relative ionic radii of the HS-LS Fe^{2+} and Mg^{2+} cations in the system, which has been investigated and systematically tabulated in previous studies (Shannon and Prewitt 1969; Shannon 1976; Hazen and Finger 1982). Previous studies have shown that in the octahedral coordination the effective ionic radius of the HS Fe^{2+} is 0.78 Å and the Mg^{2+} ion is 0.72 Å (Shannon and Prewitt 1969; Shannon 1976), indicating that the substitution of Fe^{2+} for Mg^{2+} would yield a larger unit-cell volume in the (MgFe)CO_3 system, i.e., the unit-cell volume of the magnesiosiderite [$(Mg_{0.35}Fe_{0.65})CO_3$] is 289.2 $Å^3$ while magnesite ($MgCO_3$) is 279.3 $Å^3$ (Zhang et al. 1997; Fiquet et al. 2002; Litasov et al. 2008). On the other hand, the extrapolated unit-cell volume of the LS magnesiosiderite of 265.1 $Å^3$ at ambient conditions is much smaller than the HS state counterpart, suggesting that the LS state is intrinsically more incompressible than the HS state, confirming the previously reported empirical relationship between the atomic compressibility and the ionic radii (Hazen and Finger 1982). As a result of the volume collapse, the LS magnesiosiderite also exhibits a smaller unit-cell volume than the end-member magnesite at given *P-T* conditions, showing that the effective ionic radius of the LS Fe^{2+} is thus smaller than the Mg^{2+} ion (Fig. 10) (e.g., Shannon and Prewitt 1969; Hazen and Finger 1982; Lavina et al. 2009).

To understand the stability of the magnesiosiderite at high *P-T* conditions, we have derived its volume and density differences from the $MgCO_3$ reference (Figs. 10 and 11). For the HS state, this volume difference is nearly 4% at 300 K and 3% at 1200 K before the spin transition. The volume difference decreases dramatically to about –2% for the LS state between 300 and 1200 K; that is, the LS state has a much lower volume than the end-member $MgCO_3$ counterpart. This volume difference in the LS state remains almost constant as a function of pressure, revealing that the LS state has similar incompressibility with the end-member $MgCO_3$.

Recent high *P-T* experimental and theoretical studies have reported that magnesite remains stable in the calcite structure (space group $R\bar{3}c$) at relevant *P-T* conditions of the lower

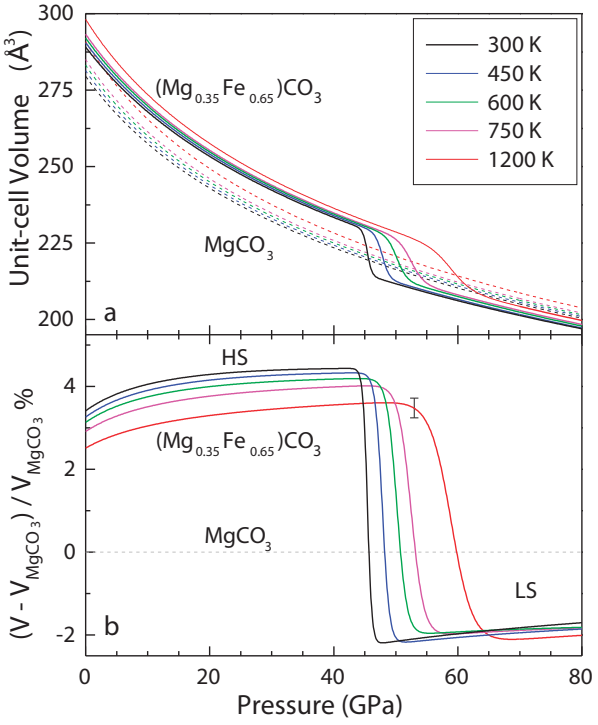

FIGURE 10. Comparison of the thermal pressure-volume relations(**a**) and volume differences (**b**) between magnesiosiderite and magnesite [$MgCO_3$] at high *P*-*T*. Solid lines in **a**: the fitted thermal *P*-*V* curves of magnesiosiderite; dashed lines: the fitted thermal *P*-*V* curves of magnesite (Zhang et al. 1997; Litasov et al. 2008). Solid lines in **b** show the volume differences across the spin transition using magnesite (V_{MgCO_3}) as the reference. Vertical ticks: representative errors. (Online color.)

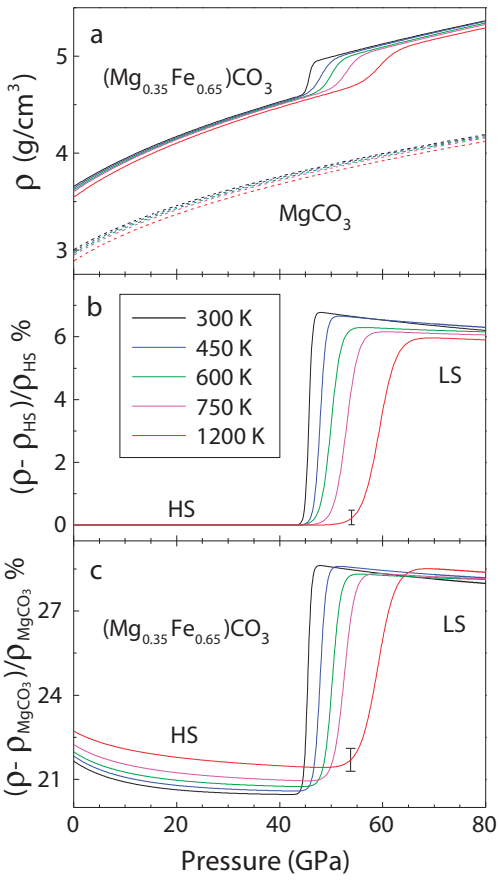

FIGURE 11. Comparison of the thermal pressure-density relations and density differences between magnesiosiderite and magnesite [$MgCO_3$] at high *P*-*T*. Solid lines in **a**: fitted thermal *P*-ρ curves of magnesiosiderite; dashed lines: fitted thermal *P*-ρ curves of magnesite (Zhang et al. 1997; Litasov et al. 2008). Solid lines in **b** show the density differences across the spin transition using the HS magnesiosiderite as the reference; Solid lines in **c** show the density differences across the spin transition using magnesite (ρ_{MgCO_3}) as the reference. Vertical ticks: representative errors. (Online color.)

mantle, instead of undergoing a dissociation that releases carbon dioxide into the surrounding mantle materials (Isshiki et al. 2004; Skorodumova et al. 2005; Oganov et al. 2008). Since the lower-mantle magnesite likely incorporates approximately 20% iron and the low-spin ferromagnesite has a smaller unit-cell volume than the high-spin counterpart, it is conceivable that the low-spin ferromagnesite can become the major deep-carbon host mineral in the lower part of the lower mantle. Specifically, extrapolations of our results show that low-spin ferromagnesite containing 20 mol% iron would be 0.6% smaller in volume and 7% denser than the end-member magnesite at relevant *P*-*T* conditions of the subducted slabs. The relatively dense low-spin ferromagnesite likely becomes more stable than the high-spin counterpart and can promote partitioning of iron into the LS state making it an even denser and much more stable phase in the lower-mantle conditions (Badro et al. 2005; Irifune et al. 2010). Detailed knowledge of the thermodynamic parameters of the whole mineralogical assemblage of the lower mantle will be needed to fully explore the thermodynamic stability of the ferromagnesite in different spin states. Future studies of physical and chemical properties of the low-spin ferromagnesite with surrounding mineral assemblages such as ferropericlase and silicate perovskite at relevant *P*-*T* conditions are still needed to understand the geophysical and geochemical consequences of the spin crossover in the lower mantle.

ACKNOWLEDGMENTS

J.F. Lin acknowledges supports from the U.S. National Science Foundation (EAR-1053446 and EAR-1056670), Deep Carbon Observatory (DCO), Energy Frontier Research Centers (EFree), and the Carnegie/DOE Alliance Center (CDAC). Synchrotron works of the study were performed at HPCAT of the APS, ANL. HPCAT is supported by CIW, CDAC, UNLV, and LLNL through funding from DOE-NNSA, DOE-BES, and NSF. APS is supported by DOE-BES, under contract no. DE-AC02-06CH11357. The authors also thank J. Wu, D. Fan, J. Yang, and B. Chen for constructive discussions.

REFERENCES CITED

Alt, J.C., and Teagle, D.A.H. (1999) The uptake of carbon during alteration of ocean crust. Geochimica et Cosmochimica Acta, 63, 1527–1535.

Angel, R.J. (2000) Equations of state. In R.M. Hazen and R.T. Downs, Eds., High-Temperature and High-Pressure Crystal Chemistry, 41, 35–59. Reviews in Mineralogy and Geochemistry, Mineralogical Society of America, Chantilly, Virginia.

Badro, J., Fiquet, G., and Guyot, F. (2005) Thermochemical state of the lower mantle: New insights from mineral physics. In R.D. van der Hilst, J.D. Bass, J. Matas, and J. Trampert, Eds., Earth's Deep Mantle: Structure, Composition, and Evolution, 160, p. 241–260. AGU, Washington, D.C.

Badro, J., Fiquet, G., Guyot, F., Rueff, J.-P., Struzhkin, V.V., Vankó, G., and Monaco, G. (2003) Iron partitioning in Earth's mantle: Toward a deep lower

mantle discontinuity. Science, 300, 789–791.
Berg, G.W. (1986) Evidence for carbonate in the mantle. Nature, 324, 50–51.
Birch, F. (1978) Finite strain isotherm and velocities for single-crystal and polycrystalline NaCl at high pressures and 300 K. Journal of Geophysical Research: Solid Earth, 83, 1257–1268.
Boulard, E., Gloter, A., Corgne, A., Antonangeli, D., Auzende, A., Perrillat, J., Guyot, F., and Fiquet, G. (2011) New host for carbon in the deep Earth. Proceedings of the National Academy of Sciences, 108, 5184–5187.
Boulard, E., Menguy, N., Auzende, A.L., Benzerara, K., Bureau, H., Antonangeli, D., Corgne, A., Morard, G., Siebert, J., Perrillat, J.P., Guyot, F., and Fiquet, G. (2012) Experimental investigation of the stability of Fe-rich carbonates in the lower mantle. Journal of Geophysical Research, 117, B02208.
Brown, J.M., and Shankland, T.J. (1981) Thermodynamic parameters in the Earth as determined from seismic profiles. Geophysical Journal of the Royal Astronomical Society, 66, 579–596.
Burns, R.G. (1993) Mineralogical Applications of Crystal Field Theory, 2nd ed. Cambridge University Press, U.K.
Crowhurst, J.C., Brown, J.M., Goncharov, A.F., and Jacobsen, S.D. (2008) Elasticity of (Mg,Fe)O through the spin transition of iron in the lower mantle. Science, 319, 451–453.
Dasgupta, R., and Hirschmann, M.M. (2010) The deep carbon cycle and melting in Earth's interior. Earth and Planetary Science Letters, 298, 1–13.
Dasgupta, R., Hirschmann, M.M., and Withers, A.C. (2004) Deep global cycling of carbon constrained by the solidus of anhydrous, carbonated eclogite under upper mantle conditions. Earth and Planetary Science Letters, 227, 73–85.
Dasgupta, R., Chi, H., Shimizu, N., Buono, A.S., and Walker, D. (2013) Carbon solution and partitioning between metallic and silicate melts in a shallow magma ocean: Implications for the origin and distribution of terrestrial carbon. Geochimica et Cosmochimica Acta, 102, 191–212.
Farfan, G., Wang, S., Ma, H., Caracas, R., and Mao, W.L. (2012) Bonding and structural changes in siderite at high pressure. American Mineralogist, 97, 1421–1426.
Fei, Y., Ricolleau, A., Frank, M., Mibe, K., Shen, G., and Prakapenka, V. (2007a) Toward an internally consistent pressure scale. Proceedings of the National Academy of Sciences, 104, 9182–9186.
Fei, Y., Zhang, L., Corgne, A., Watson, H., Ricolleau, A., Meng, Y., and Prakapenka, V. (2007b) Spin transition and equations of state of (Mg, Fe)O solid solutions. Geophysical Research Letters, 34, L17307.
Fiquet, G., Guyot, F., Kunz, M., Matas, J., Andrault, D., and Hanfland, M. (2002) Structural refinements of magnesite at very high pressure. American Mineralogist, 87, 1261–1265.
Gaillard, F., Malki, M., Iacono-Marziano, G., Pichavant, M., and Scaillet, B. (2008) Carbonatite melts and electrical conductivity in the asthenosphere. Science, 322, 1363–1365.
Hammersley, A.P., Svensson, S.O., Hanfland, M., Fitch, A.N., and Hausermann, D. (1996) Two-dimensional detector software: From real detector to idealised image or two-theta scan. High Pressure Research, 14, 235–248.
Hazen, R.M., and Finger, L.W. (1982) Comparative Crystal Chemistry, p. 165–193. Wiley-Interscience, New York.
Hazen, R.M., Hemley, R.J., and Mangum, A.J. (2012) Carbon in Earth's interior: Storage, cycling, and life. Eos, Transactions American Geophysical Union, 93, 17–18.
Irifune, T., Shinmei, T., McCammon, C.A., Miyajima, N., Rubie, D.C., and Frost, D.J. (2010) Iron partitioning and density changes of pyrolite in Earth's lower mantle. Science, 327, 193–195.
Isshiki, M., Irifune, T., Hirose, K., Ono, S., Ohishi, Y., Watanuki, T., Nishibori, E., Takata, M., and Sakata, M. (2004) Stability of magnesite and its high-pressure form in the lowermost mantle. Nature, 427, 60–63.
Kantor, I., Prakapenka, V., Kantor, A., Dera, P., Kurnosov, A., Sinogeikin, S., Dubrovinskaia, N., and Dubrovinsky, L. (2012) BX90: A new diamond anvil cell design for X-ray diffraction and optical measurements. Review of Scientific Instruments, 83, 125102.
Keppler, H., Wiedenbeck, M., and Shcheka, S.S. (2003) Carbon solubility in olivine and the mode of carbon storage in the Earth's mantle. Nature, 424, 414–416.
Keppler, H., Kantor, I., and Dubrovinsky, L.S. (2007) Optical absorption spectra of ferropericlase to 84 GPa. American Mineralogist, 92, 433–436.
Komabayashi, T., Hirose, K., Nagaya, Y., Sugimura, E., and Ohishi, Y. (2010) High-temperature compression of ferropericlase and the effect of temperature on iron spin transition. Earth and Planetary Science Letters, 297, 691–699.
Lavina, B., Dera, P., Downs, R.T., Prakapenka, V., Rivers, M., Sutton, S., and Nicol, M. (2009) Siderite at lower mantle conditions and the effects of the pressure-induced spin-pairing transition. Geophysical Research Letters, 36, L23306.
Lavina, B., Dera, P., Downs, R.T., Tschauner, O., Yang, W., Shebanova, O., and Shen, G. (2010a) Effect of dilution on the spin pairing transition in rhombohedral carbonates. High Pressure Research, 30, 224–229.
Lavina, B., Dera, P., Downs, R.T., Yang, W., Sinogeikin, S., Meng, Y., Shen, G., and Schiferl, D. (2010b) Structure of siderite $FeCO_3$ to 56 GPa and hysteresis of its spin-pairing transition. Physical Review B, 82, 064110.
Li, J. (2007) Electronic transitions and spin states in the lower mantle. In K. Hirose, J. Brodholt, T. Lay, and D. Yuen, Eds., Post-Perovskite: The Last Mantle Phase Transition, 174, p. 47–68. Geophysical Monograph Series, American Geophysical Union, Washington, D.C.
Lin, J.-F., and Tsuchiya, T. (2008) Spin transition of iron in the Earth's lower mantle. Physics of the Earth and Planetary Interiors, 170, 248–259.
Lin, J.-F., Struzhkin, V.V., Jacobsen, S.D., Hu, M.Y., Chow, P., Kung, J., Liu, H., Mao, H., and Hemley, R.J. (2005) Spin transition of iron in magnesiowüstite in the Earth's lower mantle. Nature, 436, 377–380.
Lin, J.-F., Gavriliuk, A.G., Struzhkin, V.V., Jacobsen, S.D., Sturhahn, W., Hu, M.Y., Chow, P., and Yoo, C.-S. (2006) Pressure-induced electronic spin transition of iron in magnesiowustite-(Mg,Fe)O. Physical Review B, 73, 113107.
Lin, J.-F., Weir, S.T., Jackson, D.D., Evans, W.J., Vohra, Y.K., Qiu, W., and Yoo, C.-S. (2007a) Electrical conductivity of the lower-mantle ferropericlase across the electronic spin transition. Geophysical Research Letters, 34, L16305.
Lin, J.-F., Vankó, G., Jacobsen, S.D., Iota, V., Struzhkin, V.V., Prakapenka, V.B., Kuznetsov, A., and Yoo, C. (2007b) Spin transition zone in Earth's lower mantle. Science, 317, 1740–1743.
Lin, J.-F., Liu, J., Jacobs, C., and Prakapenka, V.B. (2012) Vibrational and elastic properties of ferromagnesite across the electronic spin-pairing transition of iron. American Mineralogist, 97, 583–591.
Lin, J.-F., Speziale, S., Mao, Z., and Marquardt, H. (2013) Effects of the electronic spin transitions of iron in lower mantle minerals: Implications for deep mantle geophysics and geochemistry. Reviews of Geophysics, 51, 244–275, DOI: 10.1002/rog.20010.
Litasov, K.D., Fei, Y., Ohtani, E., Kuribayashi, T., and Funakoshi, K. (2008) Thermal equation of state of magnesite to 32 GPa and 2073 K. Physics of the Earth and Planetary Interiors, 168, 191–203.
Mao, Z., Lin, J.-F., Liu, J., and Prakapenka, V.B. (2011) Thermal equation of state of lower-mantle ferropericlase across the spin crossover. Geophysical Research Letters, 38, L23308.
Marquardt, H., Speziale, S., Reichmann, H.J., Frost, D.J., and Schilling, F.R. (2009a) Single-crystal elasticity of $(Mg_{0.9}Fe_{0.1})O$ to 81 GPa. Earth and Planetary Science Letters, 287, 345–352.
Marquardt, H., Speziale, S., Reichmann, H.J., Frost, D.J., Schilling, F.R., and Garnero, E.J. (2009b) Elastic shear anisotropy of ferropericlase in Earth's lower mantle. Science, 324, 224–226.
Mattila, A., Pylkkänen, T., Rueff, J.P., Huotari, S., Vankó, G., Hanfland, M., Lehtinen, M., and Hämäläinen, K. (2007) Pressure induced magnetic transition in siderite $FeCO_3$ studied by X-ray emission spectroscopy. Journal of Physics: Condensed Matter, 19, 386206.
Nagai, T., Ishido, T., Seto, Y., Nishio-Hamane, D., Sata, N., and Fujino, K. (2010) Pressure-induced spin transition in $FeCO_3$-siderite studied by X-ray diffraction measurements. Journal of Physics: Conference Series, 215, 012002.
Oganov, A.R., Ono, S., Ma, Y., Glass, C.W., and Garcia, A. (2008) Novel high-pressure structures of $MgCO_3$, $CaCO_3$ and CO_2 and their role in Earth's lower mantle. Earth and Planetary Science Letters, 273, 38–47.
Pal'yanov, Y.N., Sokol, A.G., Borzdov, Y.M., Khokhryakov, A.F., and Sobolev, N.V. (1999) Diamond formation from mantle carbonate fluids. Nature, 400, 417–418.
Persson, K., Bengtson, A., Ceder, G., and Morgan, D. (2006) Ab initio study of the composition dependence of the pressure-induced spin transition in the $(Mg_{1-x}, Fe_x)O$ system. Geophysical Research Letters, 33, L16306.
Prakapenka, V.B., Kubo, A., Kuznetsov, A., Laskin, A., Shkurikhin, O., Dera, P., Rivers, M.L., and Sutton, S.R. (2008) Advanced flat top laser heating system for high pressure research at GSECARS: application to the melting behavior of germanium. High Pressure Research, 28, 225–235.
Robie, R.A., Haselton, H.T., and Hemingway, B.S. (1984) Heat capacities and entropies of rhodochrosite ($MnCO_3$) and siderite ($FeCO_3$) between 5 and 600 K. American Mineralogist, 69, 349–357.
Sanchez-Valle, C., Ghosh, S., and Rosa, A.D. (2011) Sound velocities of ferromagnesian carbonates and the seismic detection of carbonates in eclogites and the mantle. Geophysical Research Letters, 38, L24315.
Shannon, R.D. (1976) Revised effective ionic radii and systematic studies of interatomic distances in halides and chalcogenides. Acta Crystallographica, A32, 751–767.
Shannon, R.D., and Prewitt, C.T. (1969) Effective ionic radii in oxides and fluorides. Acta Crystallographica, B25, 925–946.
Shi, H., Luo, W., Johansson, B., and Ahuja, R. (2008) First-principles calculations of the electronic structure and pressure-induced magnetic transition in siderite $FeCO_3$. Physical Review B, 78, 155119.
Skorodumova, N.V., Belonoshko, A.B., Huang, L., Ahuja, R., and Johansson, B. (2005) Stability of the $MgCO_3$ structures under lower mantle conditions. American Mineralogist, 90, 1008–1011.
Speziale, S., Lee, V.E., Clark, S.M., Lin, J.F., Pasternak, M.P., and Jeanloz, R. (2007) Effects of Fe spin transition on the elasticity of (Mg,Fe)O magnesiowüstites and implications for the seismological properties of the Earth's lower mantle. Journal of Geophysical Research: Solid Earth, 112, B10212.
Speziale, S., Milner, A., Lee, V.E., Clark, S.M., Pasternak, M.P., and Jeanloz, R. (2005) Iron spin transition in Earth's mantle. Proceedings of the National

Academy of Sciences, 102, 17918–17922.
Tsuchiya, T., Wentzcovitch, R.M., da Silva, C.R.S., and de Gironcoli, S. (2006) Spin transition in magnesiowüstite in Earth's lower mantle. Physical Review Letters, 96, 198501.
Wentzcovitch, R.M., Justo, J.F., Wu, Z., da Silva, C.R.S., Yuen, D.A., and Kohlstedt, D. (2009) Anomalous compressibility of ferropericlase throughout the iron spin cross-over. Proceedings of the National Academy of Sciences, 106, 8447–8452.
Wu, Z., Justo, J.F., da Silva, C.R.S., de Gironcoli, S., and Wentzcovitch, R.M. (2009) Anomalous thermodynamic properties in ferropericlase throughout its spin crossover. Physical Review B, 80, 014409.
Zhang, J., Martinez, I., Guyot, F., Gillet, P., and Saxena, S.K. (1997) X-ray diffraction study of magnesite at high pressure and high temperature. Physics and Chemistry of Minerals, 24, 122–130.
Zhang, J., Martinez, I., Guyot, F., and Reeder, R.J. (1998) Effects of Mg-Fe^{2+} substitution in calcite-structure carbonates: Thermoelastic properties. American Mineralogist, 83, 280–287.

Manuscript received March 30, 2013
Manuscript accepted August 31, 2013
Manuscript handled by Sergio Speziale